Overcoming the losses of a split ring resonator array with gain

Anan Fang,[1] **Zhixiang Huang,**[1,2] **Thomas Koschny,**[1,3] **and Costas M. Soukoulis**[1,3,*]

[1]*Department of Physics and Astronomy and Ames Laboratory, Iowa State University, Ames, Iowa 50011, USA*

[2]*Key Laboratory of Intelligent Computing and Signal Processing, Anhui University, Hefei 230039, China*

[3]*Department of Materials Science and Technology and Institute of Electronic Structure and Laser, FORTH, University of Crete, 71110 Heraklion, Crete, Greece*

**soukoulis@ameslab.gov*

Abstract: We present a computational approach, allowing for a self-consistent treatment of a split ring resonator (SRR) array with a gain layer underneath. We apply three different pumping schemes on the gain layer: (1) homogeneously pumped isotropic gain, (2) homogeneously pumped isotropic gain with a shadow cast by the SRR and (3) anisotropic gain pumped in a selected direction only. We show numerically the magnetic losses of the SRR can be compensated by the gain. The difference on loss compensations among the three pumping schemes is analyzed by the electric field distribution. Studies also show the dielectric background of gain does not affect the loss compensation much for the gain only pumped in the direction parallel to the SRR plane.

OCIS codes: (160.4760) Optical properties; (160.3918) Metamaterials; (260.5740) Resonance; (0350.4238) Nanophotonics.

References and links

1. J. B. Pendry, "Negative refraction," Contemp. Phys. **45**, 191–202 (2004).
2. S. A. Ramakrishna, "Physics of negative refractive index materials," Rep. Prog. Phys. **68**, 449–521 (2005).
3. C. M. Soukoulis, M. Kafesaki and E. N. Economou, "Negative-index materials: New frontiers in optics," Adv. Mater. **18**, 1941–1952 (2006).
4. V. M. Shalaev, "Optical negative-index metamaterials," Nature Photon. **1**, 41–48 (2007).
5. C. M. Soukoulis, S. Linden, and M. Wegener, "Negative refractive index at optical wavelengths," Science **315**, 47–49 (2007).
6. C. M. Soukoulis and M. Wegener, "Optical metamaterials–more bulky and less lossy," Science **330**, 1633–1634 (2010).
7. F. Capolino,*Theory and Phenomena of Metamaterials* (CRC Press, Taylor and Francis Group, 2009).
8. J. B. Pendry, "Negative refraction makes a perfect lens," Phys. Rev. Lett. **85**, 3966–3969 (2000).
9. D. Schurig, J. J. Mock, B. J. Justice, S. A. Cummer, J. B. Pendry, A. F. Starr, and D. R. Smith, " Metamaterial electromagnetic cloak at microwave frequencies," Science **314**, 977–980 (2006).
10. J. Zhou, Th. Koschny, and C. M. Soukoulis, "An efficient way to reduce losses of left-handed metamaterials," Opt. Express **16**, 11147–11152 (2008).
11. J. Valentine, S. Zhang, T. Zentgraf, E. Ulin-Avila, D. A. Genov, G. Bartal, and X. Zhang, "Three-dimensional optical metamaterial with a negative refractive index," Nature **455**, 376–379 (2008).
12. J. Zhou, T. Koschny, M. Kafesaki, and C. M. Soukoulis, "Negative refractive index response of weakly and strongly coupled optical metamaterials," Phys. Rev. B **80**, 035109 (2009).
13. D. O. Guney, Th. Koschny, and C. M. Soukoulis, "Reducing ohmic losses in metamaterials by geometric tailoring," Phys. Rev. B **80**, 125129 (2009).

#140436 - $15.00 USD Received 4 Jan 2011; revised 24 May 2011; accepted 2 Jun 2011; published 16 Jun 2011

14. S. A. Ramakrishna and J. B. Pendry, "Removal of absorption and increase in resolution in a near-field lens via optical gain," Phys. Rev. B **67**, 201101 (2003).
15. N. M. Lawandy, "Localized surface plasmon singularities in amplifying media," Appl. Phys. Lett. **85**, 5040–5042 (2004).
16. M. A. Noginov, G. Zhu, M. Bahoura, J. Adegoke, C. E. Small, B. A. Ritzo, V. P. Drachev, and V. M. Shalaev, "Enhancement of surface plasmons in an Ag aggregate by optical gain in a dielectric medium," Opt. Lett. **31**, 3022–3024 (2006).
17. T. A. Klar, "Negative-index metamaterials: Going optical," IEEE J. Sel. Top. Quantum Electron. **12**, 1106–1115 (2006).
18. A. K. Sarychev and G. Tartakovsky, "Magnetic plasmonic metamaterials in actively pumped host medium and plasmonic nanolaser," Phys. Rev. B **75**, 085436 (2007).
19. Y. Sivan, S. Xiao, U. K. Chettiar, A. V. Kildishev, and V. M. Shalaev, "Frequency-domain simulations of a negative-index material with embedded gain," Opt. Express **17**, 24060–24074 (2009).
20. A. D. Boardman, Yu. G. Rapoport, N. King, and V. N. Malnev, "Creating stable gain in active metamaterials," J. Opt. Soc. Am. B **24**, A53–A61 (2007).
21. A. N. Lagarkov, V. N. Kisel, and A. K. Sarychev, "Loss and gain in metamaterials," J. Opt. Soc. Am. B **27**, 648–659 (2010).
22. M. Wegener, J. Luis Garca-Pomar, C. M. Soukoulis, N. Meinzer, M. Ruther, and S. Linden, "Toy model for plasmonic metamaterial resonances coupled to two-level system gain," Opt. Express **16**, 19785–19798 (2008).
23. A. Fang, Th. Koschny, M. Wegener, and C. M. Soukoulis, "Self-consistent calculation of metamaterials with gain," Phys. Rev. B **79**, 241104 (2009).
24. A. Fang, Th. Koschny, and C. M. Soukoulis, "Lasing in metamaterial nanostructures," J. Opt. **12**, 024013 (2010).
25. A. Fang, Th. Koschny, and C. M. Soukoulis, "Self-consistent calculations of loss-compensated fishnet metamaterials," Phys. Rev. B **82**, 121102 (2010).
26. S. Wuestner, A. Pusch, K. L. Tsakmakidis, J. M. Hamm, and O. Hess, "Overcoming Losses with Gain in a Negative Refractive Index Metamaterial," Phys. Rev. Lett. **105**, 127401 (2010).
27. N. I. Zheludev, S. L. Prosvirnin, N. Papasimakis, and V. A. Fedotov, "Lasing spaser," Nat. Photonics **2**, 351–354 (2008).
28. D. J. Bergman and M. I. Stockman, "Surface plasmon amplification by stimulated emission of radiation: quantum generation of coherent surface plasmons in nanosystems," Phys. Rev. Lett. **90**, 027402 (2003).
29. M. I. Stockman, "Spasers explained," Nat. Photonics **2**, 327–329 (2008).
30. K. Tanaka, E. Plum, J. Y. Ou, T. Uchino, and N. I. Zheludev, "Multifold Enhancement of Quantum Dot Luminescence in Plasmonic Metamaterials," Phys. Rev. Lett. **105**, 227403 (2010).
31. N. Meinzer, M. Ruther, S. Linden, C. M. Soukoulis, G. Khitrova, J. Hendrickson, J. D. Olitsky, H. M. Gibbs, and M. Wegener, "Arrays of Ag split-ring resonators coupled to InGaAs single-quantum-well gain," Opt. Express **18**, 24140–24151 (2010).
32. S. Xiao, V. P. Drachev, A. V. Kildishev, X. Ni, U. K. Chettiar, H.-K. Yuan, and V. M. Shalaev, "Loss-free and active optical negative-index metamaterials," Nature **466**, 735–738 (2010).
33. A. E. Siegman, *Lasers* (Hill Valley, 1986), Chaps. 2, 3, 6, and 13.
34. A. Taflove, *Computational Electrodynamics: The Finite Difference Time Domain Method* (Artech House, London, 1995). See Chaps. 3, 6, and 7.
35. D. R. Smith, S. Schultz, P. Markoŝ, and C. M. Soukoulis, "Determination of effective permittivity and permeability of metamaterials from reflection and transmission coefficients," Phys. Rev. B **65**, 195104 (2002).
36. Th. Koschny, P. Markoŝ, E. N. Economou, D. R. Smith, D. C. Vier, and C. M. Soukoulis, "Impact of inherent periodic structure on effective medium description of left-handed and related metamaterials," Phys. Rev. B **71**, 245105 (2005).
37. N. Katsarakis, T. Koschny, M. Kafesaki, E. N. Economou, and C. M. Soukoulis, "Electric coupling to the magnetic resonance of split ring resonators," Appl. Phys. Lett. **84**, 2943–2945 (2004).
38. D. Schurig, J. J. Mock, and D. R. Smith, "Electric-field-coupled resonators for negative permittivity metamaterials," Appl. Phys. Lett. **88**, 041109 (2006).

1. Introduction

The field of metamaterials has seen spectacular experimental progress in recent years [1–7]. However, huge intrinsic losses in the metal-based structures have become the major obstacle towards real world applications at optical wavelengths. Generally, losses are orders of magnitude too large for the envisioned applications, such as, perfect lenses [8], and invisibility cloaking [9]. Achieving such reduction of losses by geometric tailoring of the metamaterial designs [10–13] appears to be out of reach. So far, the most promising and generic approach is to incorporate gain material into metamaterial designs. One important issue is not to assume

#140436 - $15.00 USD Received 4 Jan 2011; revised 24 May 2011; accepted 2 Jun 2011; published 16 Jun 2011

the metamaterial structure and the gain medium are independent from one another [14–21]. In fact, increasing the gain in the metamaterial changes the metamaterial properties, which, in turn, changes the coupling to the gain medium until a steady state is reached. So, there is a need for self-consistent calculations [22–26] for incorporating gain materials into realistic metamaterials. Instead of simply forcing negative imaginary parts of the local gain material's response function, which produces strictly linear gain, the self-consistent approach inherently includes the nonlinearity and gain saturation of the gain material. When the signal amplitudes are very weak and in the linear region of gain, the linear model can be obtained in the self-consistent approach by assuming a constant population inversion in Eq. (1), i.e., a population inversion given by an 'average field'. However, for strong signals, it is necessary to have self-consistent calculations.

Time-domain self-consistent calculations of gain incorporated into 2D magnetic metamaterials [23,24] and 3D realistic fishnet structures [25,26] have been recently reported. Results have shown the magnetic resonances of the 2D split-ring resonators (SRRs) and the fishnet structures can be substantially undamped by the gain material. Hence, the losses of the magnetic susceptibility, μ, are compensated. It is demonstrated the gain medium can give an effective gain much larger than its bulk counterpart due to the strong local-field enhancement inside the metamaterial designs [23, 27–29]. Recent experimental works also report loss compensations in metamaterial nanostructures coupled with quantum dots [30], single quantum wells [31] and organic dyes [32].

In this paper, we apply a detailed 3D self-consistent computational scheme to study the optical response of a realistic SRR array with a gain layer underneath. In section 2, we present the semi-classical theory of lasing and describe in detail the computational approach. In section 3, we present the geometric dimensions of the SRR array with gain. In section 4, we study the loss compensations of the combined SRR-gain system for three different pumping schemes on the gain layer: (1) the gain is isotropic and pumped with a homogeneous pumping rate, (2) the gain is isotropic but has a shadow cast by the SRR where the gain is away and (3) the gain is anisotropic, i.e., it is only pumped in one selected direction. In addition, we investigate the effect of the gain dielectric background on the loss compensation. In section 5, we present our conclusions.

2. Theory and model

The gain atoms are embedded in the host medium and described by a generic four-level atomic system, which tracks fields and occupation numbers at each point in space, taking into account energy exchange between atoms and fields, electronic pumping, and non-radiative decays [33]. The two-level system is not taken because in reality it can not achieve the population inversion required for gain and lasing due to the de-exciting processes of spontaneous and stimulated emssions. The four-level system is more efficient in achieving the population inversion and most practical gain media can be modeled by the system of this type. An external mechanism pumps electrons from the ground state level, N_0, to the third level, N_3, at a certain pumping rate, Γ_{pump}, proportional to the optical pumping intensity in an experiment. After a short lifetime, τ_{32}, electrons transfer non-radiatively into the metastable second level, N_2. The second level (N_2) and the first level (N_1) are called the upper and lower lasing levels. Electrons can be transferred from the upper to the lower lasing level by spontaneous and stimulated emissions. At last, electrons transfer quickly and non-radiatively from the first level (N_1) to the ground state level (N_0). The lifetimes and energies of the upper and lower lasing levels are τ_{21}, E_2 and τ_{10}, E_1, respectively. The center frequency of the radiation is $\omega_a = (E_2 - E_1)/\hbar$, chosen to equal $2\pi \times 10^{14}$ rad/s. The parameters, τ_{32}, τ_{21}, and τ_{10}, are chosen 5×10^{-14}, 5×10^{-12}, and 5×10^{-14} s, respectively. The total electron density, $N_0(t=0) = N_0(t) + N_1(t) + N_2(t) + N_3(t) = 5.0 \times$

#140436 - $15.00 USD Received 4 Jan 2011; revised 24 May 2011; accepted 2 Jun 2011; published 16 Jun 2011

$10^{23}/\mathrm{m}^3$, and the pumping rate, Γ_{pump}, is an external parameter. These gain parameters are chosen to overlap with the resonance of the split-ring resonator. The time-dependent Maxwell equations are given by $\nabla \times \mathbf{E} = -\partial \mathbf{B}/\partial t$ and $\nabla \times \mathbf{H} = \varepsilon\varepsilon_o \partial \mathbf{E}/\partial t + \partial \mathbf{P}/\partial t$, where $\mathbf{B} = \mu\mu_o \mathbf{H}$ and $\mathbf{P}$ is the dispersive electric polarization density from which the amplification and gain can be obtained. Following the single electron case, we can show [33] the polarization density $\mathbf{P}(\mathbf{r},t)$ in the presence of an electric field obeys locally the following equation of motion,

$$\frac{\partial^2 \mathbf{P}(t)}{\partial t^2} + \Gamma_a \frac{\partial \mathbf{P}(t)}{\partial t} + \omega_a^2 \mathbf{P}(t) \;=\; -\sigma_a \Delta N(t) \mathbf{E}(t), \tag{1}$$

where Γ_a is the linewidth of the atomic transition ω_a and is equal to $2\pi \times 20 \times 10^{12}\,\mathrm{rad/s}$. The factor, $\Delta N(\mathbf{r},t) = N_2(\mathbf{r},t) - N_1(\mathbf{r},t)$, is the population inversion that drives the polarization, and σ_a is the coupling strength of $\mathbf{P}$ to the external electric field and its value is taken to be $10^{-4}\,\mathrm{C}^2/\mathrm{kg}$. It follows [33] from Eq. 1 that the amplification line shape is Lorentzian and homogeneously broadened. The occupation numbers at each spatial point vary according to

$$\frac{\partial N_3}{\partial t} = \Gamma_{\mathrm{pump}} N_0 - \frac{N_3}{\tau_{32}}, \tag{2a}$$

$$\frac{\partial N_2}{\partial t} = \frac{N_3}{\tau_{32}} + \frac{1}{\hbar\omega_a} \mathbf{E} \cdot \frac{\partial \mathbf{P}}{\partial t} - \frac{N_2}{\tau_{21}}, \tag{2b}$$

$$\frac{\partial N_1}{\partial t} = \frac{N_2}{\tau_{21}} - \frac{1}{\hbar\omega_a} \mathbf{E} \cdot \frac{\partial \mathbf{P}}{\partial t} - \frac{N_1}{\tau_{10}}, \tag{2c}$$

$$\frac{\partial N_0}{\partial t} = \frac{N_1}{\tau_{10}} - \Gamma_{\mathrm{pump}} N_0, \tag{2d}$$

where $\frac{1}{\hbar\omega_a} \mathbf{E} \cdot \frac{\partial \mathbf{P}}{\partial t}$ is the induced radiation rate or excitation rate depending on its sign.

To solve the behavior of the active materials in the electromagnetic fields numerically, the finite-difference time-domain (FDTD) technique is utilized [34]. In the FDTD calculations, the discrete time and space steps are chosen to be $\Delta t = 2.0 \times 10^{-18}\,\mathrm{s}$ and $\Delta x = 2.5 \times 10^{-9}\,\mathrm{m}$. The initial condition is that all the electrons are in the ground state, so there is no field, no polarization, and no spontaneous emission. Then, the electrons are pumped from N_0 to N_3 (then relaxing to N_2) with a constant pump rate, Γ_{pump}. The system begins to evolve according to the system of equations above.

3. Geometric dimensions of the SRR array

As shown in Fig. 1(a), the SRR is fabricated on a GaAs-gain-GaAs sandwich substrate. It is made from silver with its permittivity given by a Drude model, $\varepsilon(\omega) = 1 - \omega_p^2/(\omega^2 + i\omega\gamma)$, where $\omega_p = 1.37 \times 10^{16}\,\mathrm{rad/s}$ and $\gamma = 2.73 \times 10^{13}\,\mathrm{rad/s}$. The GaAs layer between the SRR and gain is introduced to avoid the quenching effect. The incident wave propagates along the y direction parallel to the SRR plane and has the magnetic field perpendicular to that plane. The unit cell size along the propagation direction is a. In z direction, the unit cell size is h, which is larger than $h_1 + h_2 + h_3 + h_s$, where h_1, h_2, h_3 and h_s are the thicknesses of the bottom GaAs layer, the gain layer, the GaAs spacing layer, and the SRR, respectively. Along the unit cell boundaries in x and z directions, periodic boundary conditions are enforced to simulate the infinite periodic structure. All the dimensions are chosen to have the magnetic resonance overlap with the emission frequency of 100 THz of the gain material. For comparison, we also introduce another gain configuration (see Fig. 1(b)), where the gain is embedded in the gap of the SRR instead of a layer underneath. The dimensions are kept the same as Fig. 1(a).

#140436 - $15.00 USD Received 4 Jan 2011; revised 24 May 2011; accepted 2 Jun 2011; published 16 Jun 2011

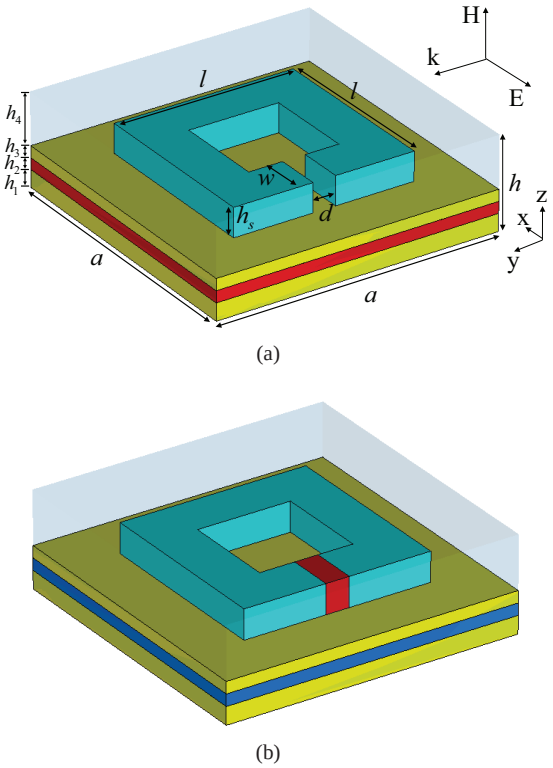

Fig. 1. (Color online) (a) One unit cell for the silver-based SRR structure (light blue) with the gain layer underneath. The dielectric constants ε for GaAs (yellow) and gain (red) are 11 and 2, respectively. The whole structure is in vacuum background (light gray). The dimensions are $a = 250\,\text{nm}$, $l = 160\,\text{nm}$, $h = 80\,\text{nm}$, $h_1 = 15\,\text{nm}$, $h_2 = h_3 = 10\,\text{nm}$, $h_4 = 45\,\text{nm}$, $h_s = 25\,\text{nm}$, $w = 40\,\text{nm}$ and $d = 20\,\text{nm}$. (b) same as (a) except the gain is embedded in the SRR gap with $\varepsilon = 1$ and the gain layer in (a) is replaced by a dielectric layer ($\varepsilon = 2$) (blue).

4. Numerical simulations and discussions

In this section, we apply the three pumping schemes discussed in section 1 on the gain layer. The linewidths of the magnetic resonances for different pumping rates are investigated to see if the gain can effectively reduce the magnetic losses. We also do simulations for different gain background dielectric constants to see how it affects the loss compensation.

4.1. Isotropic gain

We first let a wide band Gaussian pulse of a given amplitude go through one layer of the SRR structure shown in Fig. 1(a) and calculate the transmission T, the reflection R, and the absorption $A = 1 - T - R$, as a function of frequency in the propagation direction. With the introduction of gain, the absorption near the resonance frequency $f = 100\,\text{THz}$ decreases and the transmission increases. To investigate the loss reduction of the magnetic resonators, we plot the retrieved effective permeabilities, μ, without and with gain by inverting the scattering amplitudes [35, 36] in Fig. 2(a). One can see the gain undamps the magnetic resonance of the SRR and the resonant effective permeability μ of the SRR becomes much stronger and narrower compared to the case without gain. In Fig. 2(b), we plot the effective permeabilities, μ, without

#140436 - $15.00 USD Received 4 Jan 2011; revised 24 May 2011; accepted 2 Jun 2011; published 16 Jun 2011

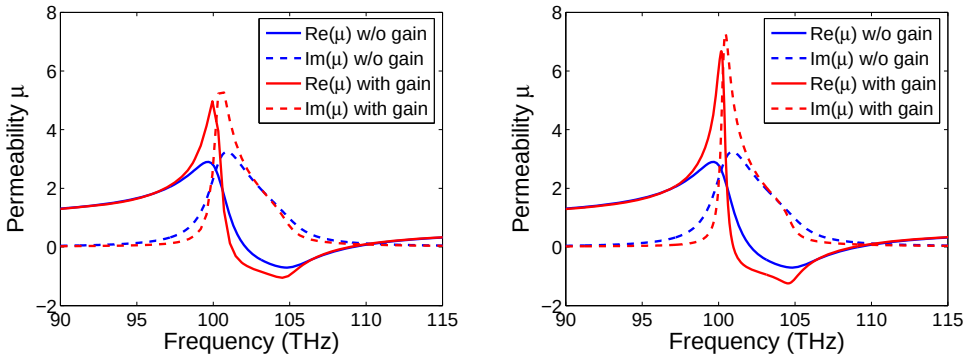

Fig. 2. (Color online) The retrieved results for the real and imaginary parts of the effective permeability μ, without and with gain, for two different gain configurations. (a) the gain is underneath the SRR as shown in Fig. 1(a). The pumping rate is $\Gamma_{\text{pump}} = 1.0 \times 10^9\,\text{s}^{-1}$. (b) the gain is in the SRR gap as shown in Fig. 1(b). The pumping rate is $\Gamma_{\text{pump}} = 7.0 \times 10^8\,\text{s}^{-1}$.

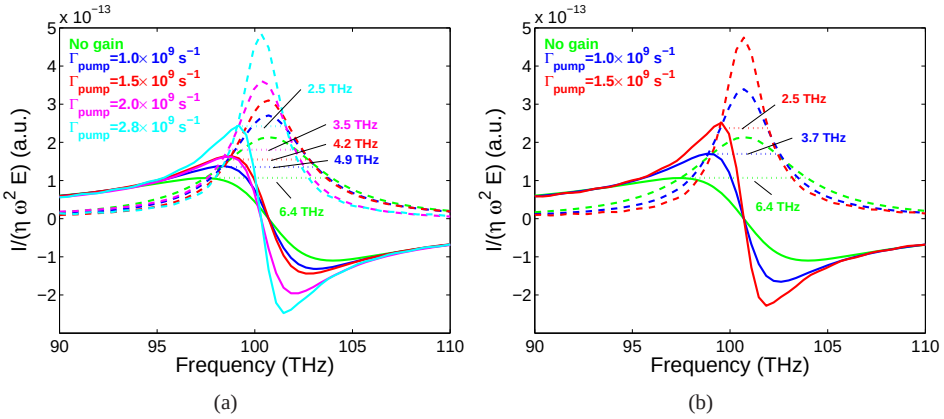

Fig. 3. (Color online) The real (solid) and imaginary (dashed) parts of $I/(\eta\omega^2 E)$ as a function of frequency for different pumping rates. (a) For the structure with a gain layer below the SRR, shown in Fig. 1(a). (b) For the structure with the gain in the SRR gap as shown in Fig. 1(b). Notice that the resonance is getting stronger and narrower as the pumping rate increases.

and with gain for the case the gain is in the SRR gap. Similar to the results for 2D SRR in Ref. 23, the weak and broad resonant μ becomes strong and narrow with the introduction of gain in the SRR gap. Note that a lower pumping rate ($\Gamma_{\text{pump}} = 7.0 \times 10^8\,\text{s}^{-1}$) leads to a sharper magnetic resonance comparing with the case the gain is underneath the SRR ($\Gamma_{\text{pump}} = 1.0 \times 10^9\,\text{s}^{-1}$) due to the local electric field concentration in the gap. However, the strong magnetic resonances in Figs. 2(a) and 2(b) are not symmetric due to the periodicity effect [36]. This asymmetry causes the difficulty in obtaining the linewidth of the magnetic resonance. The periodicity effect itself is inherent in the retrieval procedure. To distinguish the magnetic resonance of the SRR from the periodicity effect of the structure, we directly calculate the resonant current (i.e., the magnetic moment) flowing around the split ring, without going through the retrieval procedure. Consider

#140436 - $15.00 USD Received 4 Jan 2011; revised 24 May 2011; accepted 2 Jun 2011; published 16 Jun 2011

the SRR as a simple LCR circuit model, we can have the following equation,

$$L\frac{dI}{dt}+\frac{\int Idt}{C}+IR=\varepsilon_{\rm emf}, \tag{3}$$

where L, C and R are the effective inductance, capacitance and resistance of the SRR, respectively, and I is the current flowing in the SRR and $\varepsilon_{\rm emf}$ is the induced electromotive force. From Faraday's law, $\varepsilon_{\rm emf}=-d\Phi/dt=iA\mu_0\omega H=iA\frac{\omega}{c}E$. ($\Phi$ is the magnetic flux through the SRR, A is the area enclosed by SRR, and c is the speed of light in vacuum.) Then we can obtain the expression with Lorentz resonance shape,

$$\frac{I}{\eta\omega^2E}=-\frac{1}{\omega^2-\omega_0^2+i\gamma\omega}, \tag{4}$$

where η, ω_0, and γ are $A/(cL)$, $1/\sqrt{LC}$, and R/L, respectively. The detailed results are plotted in Fig. 3(a) for the structure with the gain layer underneath. One can see the current resonances have very nice Lorentz line shapes. As the pumping rate increases, the resonance is getting stronger and narrower. The full width at half maximum (FWHM) reaches 2.5 THz when the pumping rate $\Gamma_{\rm pump}=2.8\times10^9\,{\rm s}^{-1}$, which is a significant loss reduction compared with the FWHM without gain (FWHM = 6.4 THz). So the gain compensates the losses. In addition, we also calculate $I/(\eta\omega^2E)$ vs. frequency for the structure with gain in the SRR gap to compare the efficiency of the loss compensation for these two different gain configurations. The results are shown in Fig. 3(b). One can see the structure with gain in the SRR gap needs less gain (i.e., smaller pumping rate $1.5\times10^9\,{\rm s}^{-1}$) to reach the same FWHM, 2.5 THz, of the resonance than the case with gain underneath the SRR with the pumping rate $\Gamma_{\rm pump}=2.8\times10^9\,{\rm s}^{-1}$. It is easy to understand the difference in pumping rates in the two designs because of the strong local electric field enhancement in the SRR gap. Though the loss compensation for the structure with a gain layer underneath is not so efficient as the case with the gain in the SRR gap, the results in Fig. 3(a) still show that the magnetic losses can be substantially reduced, especially if we push the pumping rate to a high value.

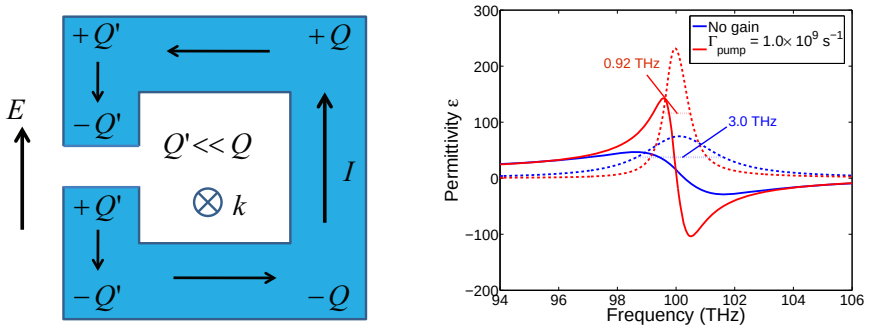

(a) (b)

Fig. 4. (Color online) (a) Schematic of the excitation of the magnetic resonance by the incident electric field **E** parallel to the gap bearing side of the SRR. A circular current appears due to the different configuration of surface charges on both sides of the SRR. (b) The retrieved results for the real (solid) and imaginary (dashed) parts of the effective permittivity ε, with and without gain, for the normal incidence in Fig. 1(a). For the case with gain, the pumping rate $\Gamma_{\rm pump}=1.0\times10^9\,{\rm s}^{-1}$.

It is experimentally difficult to have the parallel incidence for such a planar structure like the SRR array. In experiments, the SRR plane is oriented perpendicular to the incidenct wave and

#140436 - $15.00 USD Received 4 Jan 2011; revised 24 May 2011; accepted 2 Jun 2011; published 16 Jun 2011

its gap bearing side is parallel to the incident electric field. Hence, the electric field can couple to the electric dipole in the gap and induce the magnetic resonance [37, 38] (see Fig. 4(a)). Simulations are done for this case to see if the losses can be compensated by the gain layer underneath. With this incidence direction, the unit cell size in the propagation direction is h, which is much smaller than the wavelength λ ($\lambda/h = 37.5$), so the resonance is far below the Brillouin zone edge and we can ignore periodicity effect. Figure 4(b) plots the retrieved effective permittivity ε, with and without gain. Both of them have a very nice Lorentz line shape. Without gain, the resonance is broad and weak, and the FWMH is 3 THz. With the introduction of gain, the resonance becomes stronger and narrower, and the FWHM reduces to a much smaller value, 0.92 THz. So the gain compensates the losses of the SRR for perpendicular incidence.

4.2. Isotropic gain with a shadow of the SRR

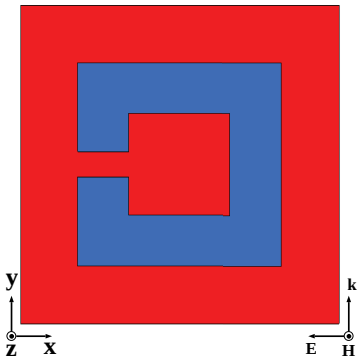

Fig. 5. Top view of the gain layer in Fig. 1(a) when a shadow (blue) is cast by the SRR structure. The gain does not exist in the shadow, while in other area (red) it is homogeneously pumped.

So far, the gain material in our simulations is isotropic and pumped by a homogeneous pumping rate Γ_{pump}. This is an ideal case. Consider the case in experiments that we incident an external optical pumping wave on the structure (Fig. 1(a)) from the top to optically pump the electrons from level 0 to level 3, there will be a shadow on the gain layer cast by the SRR structure, where the gain is pumped by a much lower rate. As a simplified model, we turn off the gain in the area which lies directly under the SRR to simply emulate the shadow of the SRR structure, while we still keep a homogeneous pumping rate Γ_{pump} in other gain area (see Fig. 5). In Fig. 6(a), we plot $I/(\eta\omega^2 E)$ as a function of frequency in this case. Compared with the case without the shadow on the gain layer (Fig. 3(a)), the resonance gets much weaker and broader (FWHM $= 5.7$ THz and 5.4 THz for the pumping rates $\Gamma_{\text{pump}} = 1.0\times10^9\,\text{s}^{-1}$ and $1.5\times10^9\,\text{s}^{-1}$, respectively). This shows the gain in the shadow area plays an important part in the loss compensation.

4.3. Anisotropic gain

The gain in our simulations discussed above is isotropic, which is equally pumped in all directions. The realistic gain, such as semiconductor quantum dots/wells, can be anisotropic, i.e., it can only couple to the external field in a certain direction. Since the electric fields in the SRR structure are mainly distributed across the gap, we have the active direction of the gain material parallel to y direction in Fig. 1(a), i.e., the gap bearing side of the SRR. So, the gain only couples to the electric field in y direction. The corresponding $I/(\eta\omega^2 E)$ vs. frequency curves for different pumping rates are plotted in Fig. 6(b). One can see the resonances are also much

#140436 - $15.00 USD Received 4 Jan 2011; revised 24 May 2011; accepted 2 Jun 2011; published 16 Jun 2011

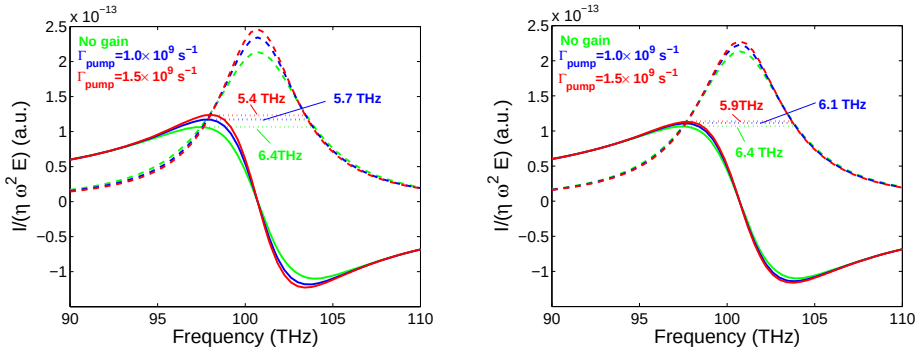

Fig. 6. (Color online) The real (solid) and imaginary (dashed) parts of $I/(\eta\omega^2 E)$ as a function of frequency for different pumping rates. (a) For the structure with a shadow on the gain layer cast by the SRR. (b) For the structure where the gain is pumped in y direction only.

broader than the case with homogeneously pumped isotropic gain. So the loss compensation is less efficient.

4.4. *Explanation of the differences among the loss compensations by the three pumping schemes*

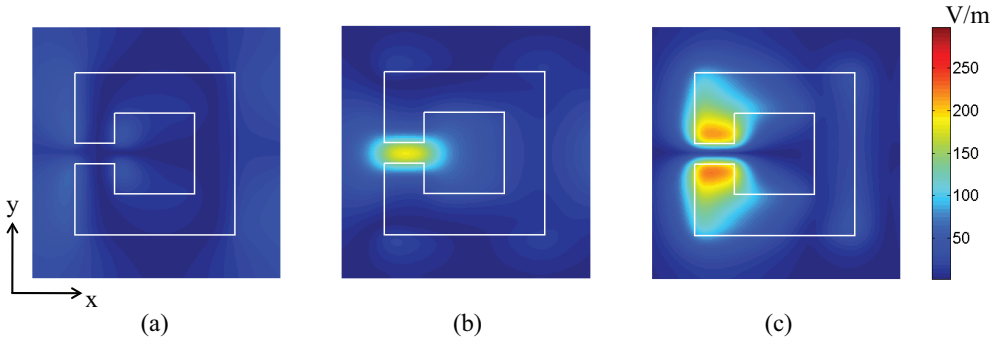

Fig. 7. (Color online) The electric field amplitude distribution at the resonance frequency in the cross-section of the gain layer ($z = 20$ nm from the bottom of the structure) for different components: (a) E_x, (b) E_y and (c) E_z. The area enclosed by the white line is the projection of the SRR on the gain layer. The electric fields are calculated without gain.

To see why these three gain pumping schemes are so different on the loss compensation, we have calculated the electric field amplitude distribution in the cross-section of the gain layer (xy plane in Fig. 1(a)). The detailed results are plotted in Figs. 7(a)–7(c). One can see the x component of electric field, E_x, is very weak while the other two components, E_y and E_z, are relatively strong. So we can ignore the gain contribution by E_x and focus on the gain from the coupling with E_y and E_z. Notice that E_y is bounded in the area right below the SRR gap (Fig. 7(b)) while E_z mainly has a significant value in the projection of the SRR on the gain layer (Fig. 7(c)). This characteristic of the field amplitude distribution leads to almost no contribution

#140436 - $15.00 USD Received 4 Jan 2011; revised 24 May 2011; accepted 2 Jun 2011; published 16 Jun 2011

by E_z when we have a shadow in the gain layer since there is no gain in that area. Similarly, the gain contribution by E_z goes away for the anisotropic gain because the gain only couples with the y component of the electric field, E_y. This fact explains the big difference between the homogeneously pumped isotropic gain and the other two gain pumping schemes.

4.5. The effect of the dielectric background of gain

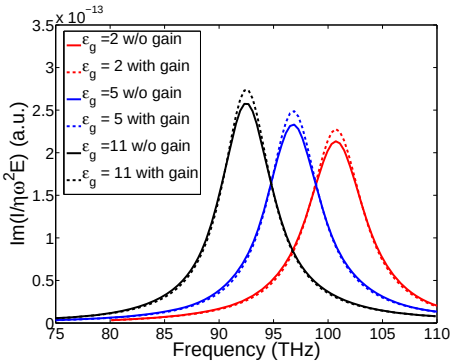

Fig. 8. (Color online) The imaginary parts of $I/(\eta\omega^2 E)$ as a function of frequency for different background dielectric constants of the gain material, which is only pumped in y direction. For the case with gain, the pumping rate is $\Gamma_{\text{pump}} = 1.5 \times 10^9\,\text{s}^{-1}$. Note the resonance enhancements by the gain are almost the same.

Since there is a high contrast between the dielectric constants of the GaAs ($\varepsilon = 11$) and gain ($\varepsilon = 2$) layers, the electromagnetic fields may be bounded in the high dielectric layer. In this section, we will discuss the effect of the dielectric background of gain on the loss compensation. In Fig. 8, we plot the detailed results for the imaginary parts of $I/(\eta\omega^2 E)$ as a function of frequency, with and without gain, for the background dielectric constants of the gain layer $\varepsilon_g = 2$, 5 and 11. The gain is anisotropic and only couples to the electric field in y direction. We can see the resonance frequency shifts down as the dielectric constant increases. This is expected since the effective capacitance increases with the increment of the dielectric constant. To effectively compensate the losses, we scale the emission frequency to overlap with the corresponding resonance frequencies and then pump with the same rate $\Gamma_{\text{pump}} = 1.5 \times 10^9\,\text{s}^{-1}$. We can see from Fig. 8 the resonance enhancements are almost the same for different background dielectric constants of the gain.

To explain this phenomenon, we plot the electric field amplitude distributions in a plane crossing the middle of the gap bearing side of the SRR (Fig. 9), for $\varepsilon_g = 2$, 5 and 11, respectively. The E_x component is ignored since it is very weak as shown in Fig. 7(a). From Fig. 9(a), we can see the field amplitude distribution of E_y, the only component which couples to the gain, does not change much in the gain layer as the gain background dielectric constant changes. Although there is a bounding effect on the fields, the y component of the electric field, E_y, does not substantially decay in such a very narrow gain layer (10 nm) neighboring to the high dielectric GaAs layer. The main change in the electric field is the z component of the electric field, E_z, decreases in the gain layer as the gain background dielectric constant, ε_g, increases, as shown in Fig. 9(b). This is due to the continuity of the normal component of the electric displacement across the interface since there is no free charge accumulation. Hence the normal component of the electric field is inversely proportional to the dielectric constant. The change of E_z does not affect the loss compensation due to no coupling between the gain and E_z. If the gain can couple

#140436 - $15.00 USD Received 4 Jan 2011; revised 24 May 2011; accepted 2 Jun 2011; published 16 Jun 2011

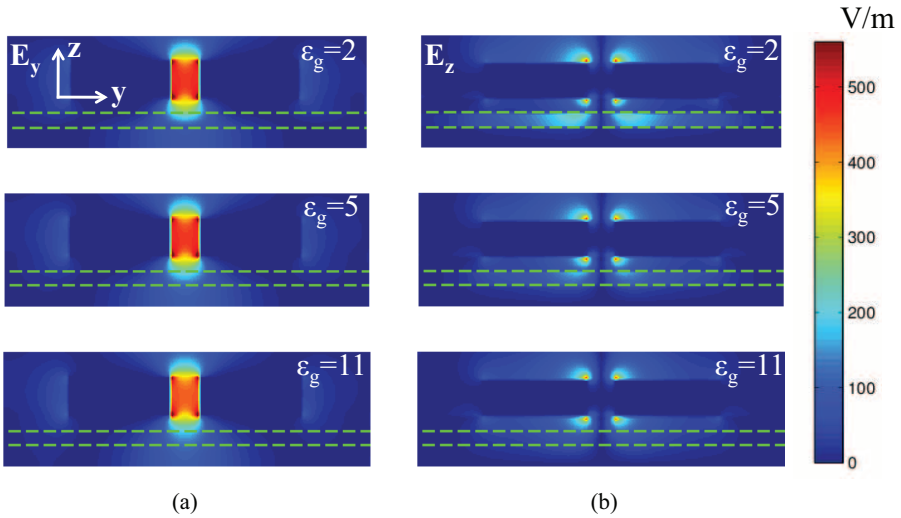

Fig. 9. (Color online) The electric field amplitude distributions for different background dielectric constants of the gain material ($\varepsilon_g = 2, 5$ and 11) at their corresponding resonance frequencies, in a *yz* plane crossing the middle of the gap bearing side of the SRR. (a) E_y and (b) E_z. The area enclosed by the dashed green line indicates the position of the gain layer. The electric fields are calculated without gain.

to E_z, such as the isotropic gain, the background dielectric constant of the gain will significantly affect the loss compensation.

5. Conclusions

We have numerically studied the loss compensation of the silver-based SRR structure with a gain layer underneath. Numerical results show that the losses of the SRR can be compensated by the gain layer for both the parallel and perpendicular incidences. Three different gain pumping schemes are applied in the simulations and the efficiencies of their corresponding loss compensations are studied by investigating the linewidth of the resonant current. The homogeneously pumped isotropic gain can significantly reduce the magnetic losses, though it is less efficient in the loss compensation compared to the case with the gain in the SRR gap. The other two schemes, (1) a homogeneously pumped isotropic gain with a shadow cast by the SRR and (2) anisotropic gain only coupled to E_y, the electric field component parallel to the gap bearing side of the SRR, are much less efficient in the loss compensation compared to the isotropic gain case, due to no interactions between the electric field perpendicular to the SRR plane, E_z, and the gain in these two schemes. We have also studied the effect of the background dielectric of gain. In a very narrow gain layer, the gain dielectric background mainly affects the electric field perpendicular to the GaAs-gain interface due to the continuity of the normal component of the electric displacement across the interface. So, the dielectric background of gain does not make much difference for the gain pumped in the parallel direction only.

Acknowledgments

Work at Ames Laboratory was supported by the Department of Energy (Basic Energy Sciences) under Contract No. DE-AC02-07CH11358. This work was partially supported by the European Community FET project PHOME (Contract No. 213390) and by Laboratory-Directed Research and Development Program at Sandia National Laboratories. The author Z. Huang

#140436 - $15.00 USD Received 4 Jan 2011; revised 24 May 2011; accepted 2 Jun 2011; published 16 Jun 2011

gratefully ackowledges support of the National Natural Science Foundation of China (Grant No. 60931002).

#140436 - $15.00 USD Received 4 Jan 2011; revised 24 May 2011; accepted 2 Jun 2011; published 16 Jun 2011